applied sciences

MDPI

Article

Quantitative Detection of Full-Circumferential Localized Corrosion in Pipes Using Longitudinal Guided Waves

Yang Liu [1,*], Hao Huang [1,2,3], Linyuan Sun [1], Xin Feng [4] and Gaixin Chen [1,2,3]

[1] China Institute of Water Resources and Hydropower Research, Beijing 100038, China
[2] State Key Laboratory of Water Cycle and Water Security, China Institute of Water Resources and Hydropower Research, Beijing 100038, China
[3] Key Laboratory of Water Engineering Materials of Ministry of Water Resources, China Institute of Water Resources and Hydropower Research, Beijing 100038, China
[4] School of Infrastructure Engineering, Dalian University of Technology, Dalian 116024, China
* Correspondence: liuy@iwhr.com; Tel.: +86-18525376080

Abstract

Localized corrosion leads to a local reduction in wall thickness in pipes, compromising their load-bearing capacity. In this study, a quantitative detection method for full-circumferential localized corrosion in pipes based on longitudinal guided waves is proposed. Based on theoretical analysis of the interaction between full-circumferential localized corrosion defects and longitudinal guided waves, the proposed method consists of two procedures. First, the theoretical relationship between the time-of-flight (TOF) difference of L(0,2) modes reflected from the front and back edges of the corrosion defect and the axial length of the corrosion defect was established using the pulse-echo method, enabling quantitative evaluation of the axial length. Subsequently, with the axial length determined, the theoretical relationship between the TOF variation of the L(0,1) mode and the depth of the corrosion defect was established using the pitch-catch method, allowing quantitative estimation of the depth. The effectiveness of this method was verified experimentally. The results demonstrate that the measured axial lengths and depths agree well with the preset values, with maximum relative errors of −1.27% and 9.52%, respectively. The proposed method overcomes the limitation of conventional guided wave methods, which are generally difficult to accurately quantify the axial length and depth of full-circumferential localized corrosion defects simultaneously.

Keywords: pipes; full-circumferential localized corrosion; longitudinal guided wave; time-of-flight (TOF); quantitative detection

Check for updates

Academic Editor: Marco Zucca

Received: 23 August 2026
Revised: 19 September 2026
Accepted: 24 September 2026
Published: 27 September 2026

Copyright: © 2026 by the authors. Licensee MDPI, Basel, Switzerland. This article is an open access article distributed under the terms and conditions of the Creative Commons Attribution (CC BY) license.

1. Introduction

Pipes are one of the primary means for long-distance transportation of water, oil, natural gas, and other resources due to their large transport capacity, low cost, high safety, and adaptability to complex terrains [1–3]. As essential infrastructure for water and energy transmission, pipe safety directly affects industrial production, daily life, and public security. However, pipes are often exposed to harsh service environments, such as humid and saline conditions, leading to inevitable corrosion degradation during long-term operation, including general and localized corrosion [4,5]. Localized corrosion is one of the most common corrosion forms in pipes and can be classified into full-circumferential and part-circumferential defects according to its circumferential extent [6,7]. Such defects cause local reductions in wall thickness, decrease load-bearing capacity, and induce stress

concentration. Once corrosion degradation exceeds a critical level, pipe failure may occur, resulting in leakage, rupture, or even catastrophic accidents. Therefore, quantitative characterization of localized corrosion defects is of great importance for ensuring pipe integrity and operational safety.

The initiation and propagation of localized corrosion in pipes are dynamic processes affected by multiple factors, making corrosion development difficult to predict. Factors such as temperature, corrosive medium composition, and stress can accelerate corrosion rates, increasing the risk of through-wall penetration and rupture. Moreover, localized corrosion defects may occur in concealed or inaccessible areas, further increasing inspection difficulties. Conventional techniques, including ultrasonic testing, magnetic flux leakage, eddy current, and X-ray, have been widely used for pipe corrosion detection [8–11]. However, these methods typically require direct access to pipes for local scanning or point-by-point inspection, resulting in low efficiency and limitations in detecting defects in inaccessible areas. They are also unsuitable for continuous and comprehensive inspection of long-distance pipes.

Ultrasonic guided wave (UGW) technology employs piezoelectric transducers to excite guided waves in structures. By analyzing variations in guided wave signals caused by corrosion and other defects, structural damage can be actively detected. Currently, UGW technology has been successfully applied to damage detection in various structures, including steel rods [12], bolts [13], steel bars [14], beams [15], plates [16], and composite structures [17]. Owing to its long propagation distance and high inspection efficiency, UGW technology enables remote detection of physically inaccessible regions [18–21]. Guided waves generate acoustic fields throughout the entire wall thickness of the pipe, allowing a small number of transducers installed at a single inspection location to evaluate a relatively large region of pipe structures. Therefore, UGW technology is highly suitable for comprehensive corrosion detection of long-distance pipes.

Extensive studies have been conducted worldwide on pipe defect detection using UGW techniques. Cawley et al. [22] investigated the effects of defect axial length on the reflection coefficients of L(0,1) and L(0,2) modes at full-circumferential axisymmetric defects and part-circumferential defects. Zhu et al. [23] analyzed the reflection characteristics and mode conversions of L(0,1) and L(0,2) modes at full-circumferential axisymmetric corrosion defects and part-circumferential non-axisymmetric corrosion defects. Demma et al. [24] studied the effects of circumferential size, axial length, and depth of pipe defects on the reflection coefficient of the T(0,1) mode. Zhang et al. [25] employed time-reversal techniques to fuse and focus defect signals, improving the signal-to-noise ratio and enabling reliable detection of through-hole defects behind pipe support structures. Zhang et al. [26] proposed a pipe damage localization method combining time-of-flight (TOF) compensation with probabilistic reconstruction, where TOF was used as a characteristic parameter to establish a circular probability distribution for circumferential localization of pipe damage. Wang et al. [27] excited the L(0,2) mode in pipes and used the Hilbert–Huang transform to extract the front-edge and back-edge reflection signals of full-circumferential corrosion defects. The time shifts between the two reflected signals were calculated to quantify the axial length of full-circumferential corrosion defects.

The existing UGW methods are mostly limited to qualitative or semi-quantitative assessments of the depth of local corrosion, and the quantitative relationship model between the depth of local corrosion and the evaluation index has not yet been theoretically developed. Moreover, conventional UGW methods based on a single evaluation parameter generally have difficulty in simultaneously and accurately quantifying both the axial length and depth of localized corrosion defects in pipes. In this study, an innovative detection method based on longitudinal guided waves is proposed for quantifying full-

circumferential localized corrosion defects in pipes. The interaction mechanisms between L(0,1) and L(0,2) modes and full-circumferential localized corrosion defects in pipes are analyzed theoretically; based on this, a dual-mode detection strategy combining the pulse-echo method and pitch-catch method is developed. Firstly, based on the pulse-echo method, the theoretical relationship between the TOF difference of the L(0,2) modes reflected from the front-edge and back-edge of the corrosion defect and the axial length of the corrosion defect is established to quantify the axial length of the corrosion defect. Subsequently, with the axial length of the corrosion defect determined, based on the pitch-catch method, the theoretical relationship between the TOF variation of the L(0,1) mode and the depth of the corrosion defect is established to quantify the depth of the corrosion defect. The coupled effects of the axial length and depth of the corrosion defect on a single parameter are theoretically decoupled using the propagation characteristics of these two longitudinal modes, thereby enabling the simultaneous and accurate quantification of both the axial length and depth of the corrosion defect. The effectiveness of the proposed method is verified through experiments.

2. Detection Principle

2.1. Propagation Characteristics of Ultrasonic Guided Waves in Pipes

When ultrasonic guided waves propagating along pipes encounter localized corrosion defects, their propagation characteristics are altered. By analyzing the variations in guided wave signals induced by localized corrosion, corrosion defects in pipes can be actively identified. The propagation of cylindrical guided waves in pipes is governed by Navier's displacement equation:

$$\mu\nabla^2 u + (\lambda + \mu)\nabla(\nabla \cdot u) = \rho\frac{\partial^2 u}{\partial t^2} \tag{1}$$

where ∇^2 denotes the Laplace operator; u and t represent the displacement vector and time, respectively; λ and μ are the Lamé constants of the pipe material; and ρ is the density of the pipe material; ∇ is the del operator; it is first used to calculate the divergence of the displacement u, i.e., $(\nabla \cdot u)$, and then to calculate the gradient of $(\nabla \cdot u)$, i.e., $\nabla(\nabla \cdot u)$. According to the work of Gazis [28], the solution of Equation (1) can be transformed into solving the dispersion equation of cylindrical guided waves in pipes, which is expressed as follows:

$$|C| = 0 \tag{2}$$

where $C = [c_{ij}]$ is a 6 × 6 matrix, and the matrix element c_{ij} is a function of multiple parameters such as the inner radius a and outer radius b of the pipe, density ρ, frequency f, and Lamé constants λ and μ. The expression of equation (2) is complex, and the detailed derivation process and complete expression can be found in reference [28]. The solutions to Equation (2) include axisymmetric longitudinal and torsional modes, as well as non-axisymmetric flexural modes. These three modes can be represented by L(0, m), T(0, m), and F(n, m), respectively; the letters L, T, and F denote longitudinal, torsional, and flexural modes, respectively; n and m are the circumferential order and the mode number, respectively; for axisymmetric modes, the circumferential order n = 0. Guided wave modes can be characterized by the dispersion curves of the group velocity and phase velocity of the guided wave. The dispersion curves of the group velocity and phase velocity of guided waves can be obtained by numerically solving Equation (2) using the Disperse program [29], which can be used for mode analysis and frequency selection. The theoretical relationship between the group velocity and phase velocity of a guided wave is as follows [30]:

$$C_g = C_p^2\left[C_p - (fd)\frac{\mathrm{d}C_p}{\mathrm{d}(fd)}\right]^{-1} \tag{3}$$

where C_g and C_p are the group velocity and phase velocity of the guided wave, respectively; fd is the frequency-thickness product, f is the frequency, and d is the wall thickness of the pipe.

Since different guided wave modes may exhibit different sensitivities to the same defect, and the sensitivity of a given mode to the same damage may also vary with frequency, selecting appropriate modes and frequencies is essential for quantitative evaluation of full-circumferential localized corrosion defects. Figure 1 shows the group velocity dispersion curves of guided waves in a steel pipe with an outer diameter of 59 mm and a wall thickness of 7 mm, in the frequency range of 0–150 kHz and for circumferential order $n \leq 3$.

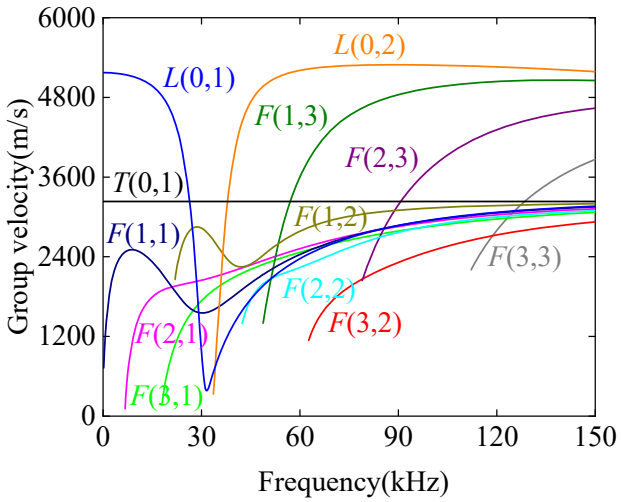


Figure 1. Group velocity dispersion curves of guided waves in the pipe.

As shown in Figure 1, at about 60–130 kHz, the L(0,2) mode is approximately non-dispersive, and the group velocity of the L(0,2) mode is much higher than that of the L(0,1) mode. Thus, the group velocity of the L(0,2) mode is basically not affected by changes in the wall thickness of the pipe in this frequency range; when this L(0,2) mode encounters corrosion defects, the reflected L(0,2) mode can reach the receiving transducer the fastest, making it easier to effectively separate it from other defect echoes in the time domain, which facilitates signal interpretation and analysis. Therefore, the L(0,2) mode in this frequency range is selected to detect the axial length of full-circumferential corrosion defects. The TOF difference of L(0,2) modes reflected for the first time from the front-edge and back-edge of the corrosion defect is related to the axial length of the corrosion defect, and the axial length of the corrosion defect can be identified using the TOF difference. The L(0,1) mode is basically dispersive in the whole frequency range, so its group velocity is affected by the change in wall thickness of the pipe. When the excitation frequency is lower than the cutoff frequency of the L(0,2) mode, a pure L(0,1) mode can be effectively excited. Consequently, the L(0,1) mode is selected for detecting the depth of a corrosion defect within the frequency range below the cutoff frequency of the L(0,2) mode. The wall thickness reduction caused by the corrosion defect will change the TOF of the L(0,1) mode, and the depth of the corrosion defect can be identified using the TOF variation of the L(0,1) mode.

2.2. Quantitative Evaluation of Axial Length and Depth of Corrosion Defect

2.2.1. Quantitative Characterization of Axial Length of Corrosion Defect

Figure 2 illustrates the interaction between the L(0,2) mode and the corrosion defect. When the excited L(0,2) mode propagates along the pipe and encounters the front-edge and back-edge of the corrosion defect, defect echoes are generated from both locations. The L(0,2) modes reflected for the first time from the front-edge and back-edge of the

corrosion defect are defined as reflected wave 1 and reflected wave 2, respectively. Based on the pulse-echo method, the difference between the TOF of reflected wave 1 and reflected wave 2 reaching the receiving array is related to the axial length of the corrosion defect. The theoretical relationship between them is expressed as follows:

$$L_c = \frac{C_{g2}\left(t_b - t_f\right)}{2} = \frac{C_{g2}\Delta t_{bf}}{2} \quad (4)$$

where L_c is the axial length of the corrosion defect, C_{g2} is the group velocity of the L(0,2) mode, t_f and t_b are the TOFs of reflected wave 1 and reflected wave 2, respectively, and Δt_{bf} represents the TOF difference between the two reflected signals. Equation (4) indicates that the axial length of the corrosion defect is positively correlated with the TOF difference of L(0,2) modes reflected from the front-edge and back-edge of the corrosion defect. By calculating the TOF difference from the measured guided wave signals and substituting it into Equation (4), the axial length of the corrosion defect can be quantitatively determined. Therefore, the proposed theoretical relationship enables quantitative characterization of the axial length of the corrosion defect.

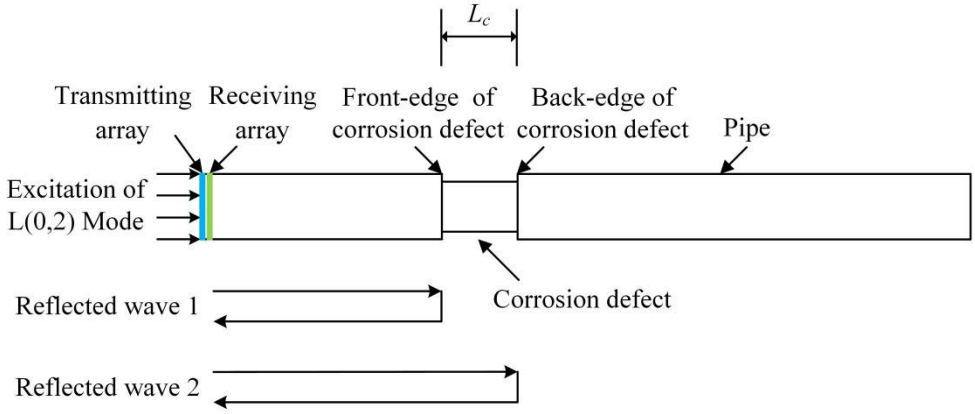


Figure 2. Interaction between the L(0,2) mode and the corrosion defect.

2.2.2. Quantitative Characterization of Depth of Corrosion Defect

As shown in Figure 1, when the frequency is less than approximately 33.62 kHz, only the L(0,1) mode exists among the longitudinal modes, and it is essentially dispersive. Equations (2) and (3) indicate that the group velocity of the guided wave is a function of frequency and the wall thickness of the pipe. Since the group velocity of the L(0,1) mode in the dispersion range is affected by changes in the wall thickness of the pipe, the L(0,1) mode within this frequency range is selected to detect the depth of the corrosion defect. Since Equation (2) is an implicit transcendental equation, it is difficult to obtain an explicit analytical solution, making it difficult to intuitively reveal the variation law of the group velocity of the L(0,1) mode with decreasing wall thickness. Fortunately, the dispersion curves of the group velocity and phase velocity of the L(0,1) mode in a pipe with a given wall thickness can be obtained directly by solving Equation (2) using the Disperse program. By analyzing the dispersion curves of the group velocity of the L(0,1) mode for various wall thicknesses of the pipe, the variation law of the group velocity of the L(0,1) mode with the decrease in the wall thickness of the pipe can be intuitively obtained.

The localized corrosion defects on the outside of the pipe lead to the thinning of the pipe wall thickness in this area, resulting in a change in the propagation characteristics of the L(0,1) mode passing through the corrosion defects. Figure 3 shows the group velocity dispersion curves of the L(0,1) mode for wall thicknesses ranging from 7 mm to 3 mm. The results indicate that within the selected frequency range, the group velocity of the L(0,1)

mode at a fixed frequency increases as the pipe wall thickness decreases. Consequently, for a given excitation frequency and axial length of the corrosion defect, the TOF of the L(0,1) mode decreases as corrosion depth increases.

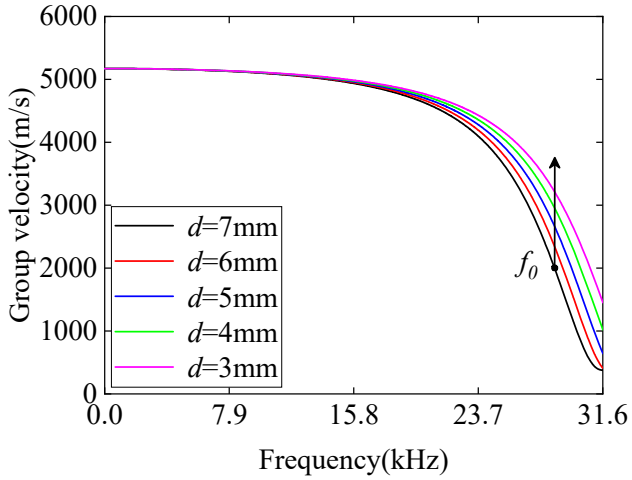


Figure 3. Group velocity dispersion curves of L(0,1) modes for different wall thicknesses.

To investigate the sensitivity of the group velocity of the L(0,1) mode to wall thickness loss of the pipe at different frequencies, the difference in the group velocity of the L(0,1) mode is calculated for wall thicknesses of 6 mm and 7 mm, and the change in the group velocity of the L(0,1) mode caused by wall thickness loss of 1 mm at different frequencies is obtained, as shown in Figure 4. In the frequency range of 0–29.6 kHz, the sensitivity of the group velocity of the L(0,1) mode to wall thickness loss increases with the increase of frequency. However, in the frequency range of 29.6–31.6 kHz, the sensitivity of the group velocity of the L(0,1) mode to wall thickness loss decreases with an increase in frequency. At 29.6 kHz, the group velocity of the L(0,1) mode is most sensitive to wall thickness loss. Based on the pitch-catch method, within the frequency range below the cutoff frequency of the L(0,2) mode and where the group velocity of the L(0,1) mode is affected by the corrosion depth, a suitable frequency is selected as the center frequency of the excitation signal to excite a pure L(0,1) mode in the pipe. Compared with an intact pipe, the TOF of the L(0,1) mode will change after passing through a full-circumferential localized corrosion defect. Therefore, the depth of a full-circumferential localized corrosion defect can be quantitatively evaluated by measuring the TOF variation of the L(0,1) mode.

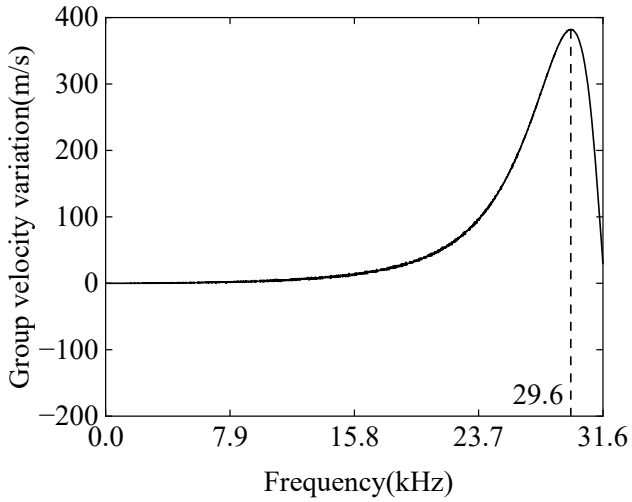


Figure 4. Group velocity variation curve of the L(0,1) mode.

To establish an accurate theoretical relationship between the depth of a full-circumferential localized corrosion defect and the TOF variation of the L(0,1) mode, the initial outer radius b_h and the corroded outer radius b_c of the pipe at the defect location are substituted into Equation (2). By numerically solving Equation (2), the group velocity dispersion curves corresponding to the initial wall thickness d_h and the wall thickness d_c after corrosion at the corrosion defect location are obtained; the group velocities of the L(0,1) mode at a selected frequency are then extracted as C_{gh} and C_{gc}, respectively. The relationship between the depth Δd_c of a full-circumferential localized corrosion defect and the induced TOF variation Δt_c of the L(0,1) mode is expressed as follows:

$$\left.\begin{array}{l} \Delta d_c = b_h - b_c = d_h - d_c \\ \Delta t_c = t_h - t_c = L_c\left(\frac{1}{C_{gh}} - \frac{1}{C_{gc}}\right) \end{array}\right\} \quad (5)$$

where t_h and t_c represent the TOFs of the L(0,1) mode before and after pipe corrosion, respectively. Equation (5) indicates that the TOF variation Δt_c of the L(0,1) mode can be used to evaluate the depth Δd_c of the corrosion defect, and this TOF variation Δt_c is related to both the axial length L_c and depth Δd_c of the corrosion defect. To establish the theoretical relationship between the TOF variation Δt_c of the L(0,1) mode and the depth Δd_c of the corrosion defect, the axial length L_c of the corrosion defect should be determined first. Firstly, the axial length L_c of the corrosion defect is calculated using Equation (4), and the measured axial length L_c of the corrosion defect is substituted into Equation (5). Subsequently, with the axial length L_c of the corrosion defect determined, the dispersion curves of the L(0,1) mode for various wall thicknesses are generated by numerically solving Equation (2), and the theoretical TOF variations of the L(0,1) mode caused by different depths of the corrosion defect are calculated using Equation (5). Finally, based on the calculated theoretical TOF variations of the L(0,1) mode and the corresponding different depths of the corrosion defect, the theoretical relationship model between the TOF variation Δt_c of the L(0,1) mode and the depth Δd_c of the corrosion defect is further established. By combining the TOF variation Δt_c of the L(0,1) mode obtained from the measured signals with the established theoretical relationship model, the depth Δd_c of the corrosion defect corresponding to the TOF variation Δt_c can be calculated. Taking the excitation frequency of 28.5 kHz, the depth of the corrosion defect increasing from 0.2 to 5.4 mm, and the axial length of the corrosion defect of 200 mm as an example, the theoretical relationship curve between the TOF variation of the L(0,1) mode and the depth of the corrosion defect is established. As shown in Figure 5, on the premise that the axial length of the corrosion defect has been determined, the TOF variation of the L(0,1) mode at a fixed frequency exhibits a positive correlation with the depth of the corrosion defect. Therefore, the theoretical relationship model enables quantitative evaluation of the depth of full-circumferential corrosion defects in pipes.

2.2.3. Quantitative Detection Scheme for Corrosion Defect in Pipes

In actual corrosion detection in pipes, to effectively evaluate the dimensions of full-circumferential corrosion defects in pipes, it is necessary to simultaneously quantify the axial length and depth of these corrosion defects. A fusion strategy combining the pulse-echo and pitch-catch methods is proposed, and a quantitative detection scheme for full-circumferential localized corrosion defects in the pipe is designed, as shown in Figure 6. A transmitting array is installed on the pipe; receiving array 1 is located at the right side of the transmitting array and is used to collect the L(0,2) modes reflected from the front-edge and back-edge of the corrosion defect, while receiving array 2 is located on the opposite side of the corrosion defect and is used to collect the L(0,1) modes passing through the

corrosion defect. A single transmitting array is employed. The L(0,1) and L(0,2) modes can be excited by switching excitation signals.

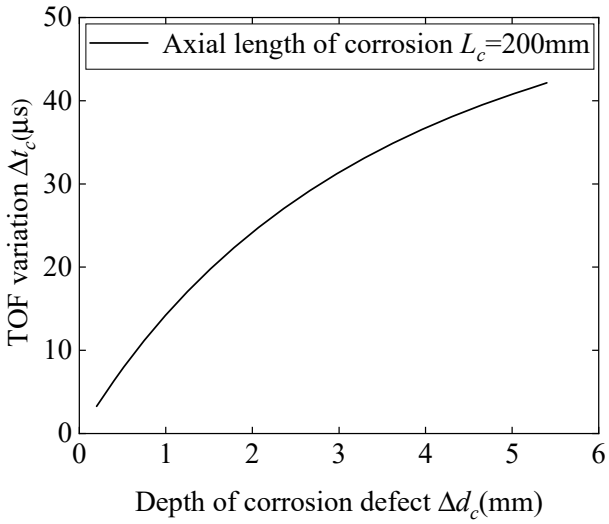


Figure 5. Theoretical relationship between TOF variation of the L(0,1) mode and the depth of corrosion defect.

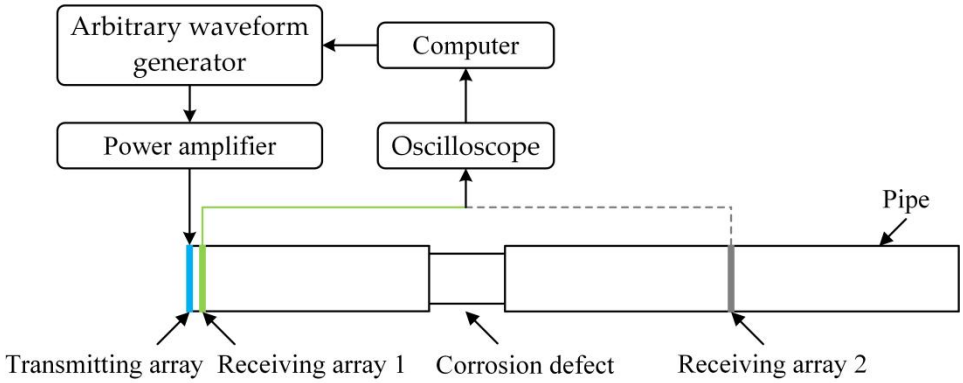


Figure 6. Schematic diagram of the quantitative detection scheme of a full-circumferential localized corrosion defect in the pipe.

Figure 7 illustrates the process for quantitative detection of a full-circumferential localized corrosion defect in the pipe. The detection process mainly involves two steps: firstly, based on the pulse-echo method, the L(0,2) mode is excited in the pipe using the transmitting array, and the L(0,2) modes reflected from the front-edge and back-edge of the corrosion defects are collected using the receiving array 1. The axial length of the corrosion defect is quantified using the method proposed in Section 2.2.1. Then, with the axial length already measured, based on the pulse-echo method, the L(0,1) mode is excited in the pipe using the transmitting array, and the L(0,1) modes passing through the corrosion defect are collected using the receiving array 2. The depth of the corrosion defect is quantified using the method proposed in Section 2.2.2.

The proposed method mainly uses TOF to evaluate the axial length and depth of the corrosion defect, so the accuracy of TOF extraction is crucial. To accurately determine TOFs of reflected wave 1 and reflected wave 2, the received guided wave signal is first band-pass filtered to reduce noise interference, and then the energy envelope of the guided wave signal is obtained using the Hilbert transform [31]. By extracting the moments corresponding to the envelope peaks at the two reflected waves, the TOFs of reflected wave 1 and reflected wave 2 are calculated separately, and the TOF difference between reflected wave 1 and

reflected wave 2 is obtained. Since the L(0,1) mode is dispersive within the excitation frequency range, to accurately extract the TOF of the L(0,1) mode at the center frequency, the received guided wave signal is first band-pass filtered to reduce noise interference. Then, a continuous wavelet transform [32] with high time-frequency resolution is used to perform time-frequency analysis on the guided wave signal, thereby extracting the TOF of the L(0,1) mode at the center frequency and obtaining the TOF variation of the L(0,1) mode under different depths of corrosion defects.

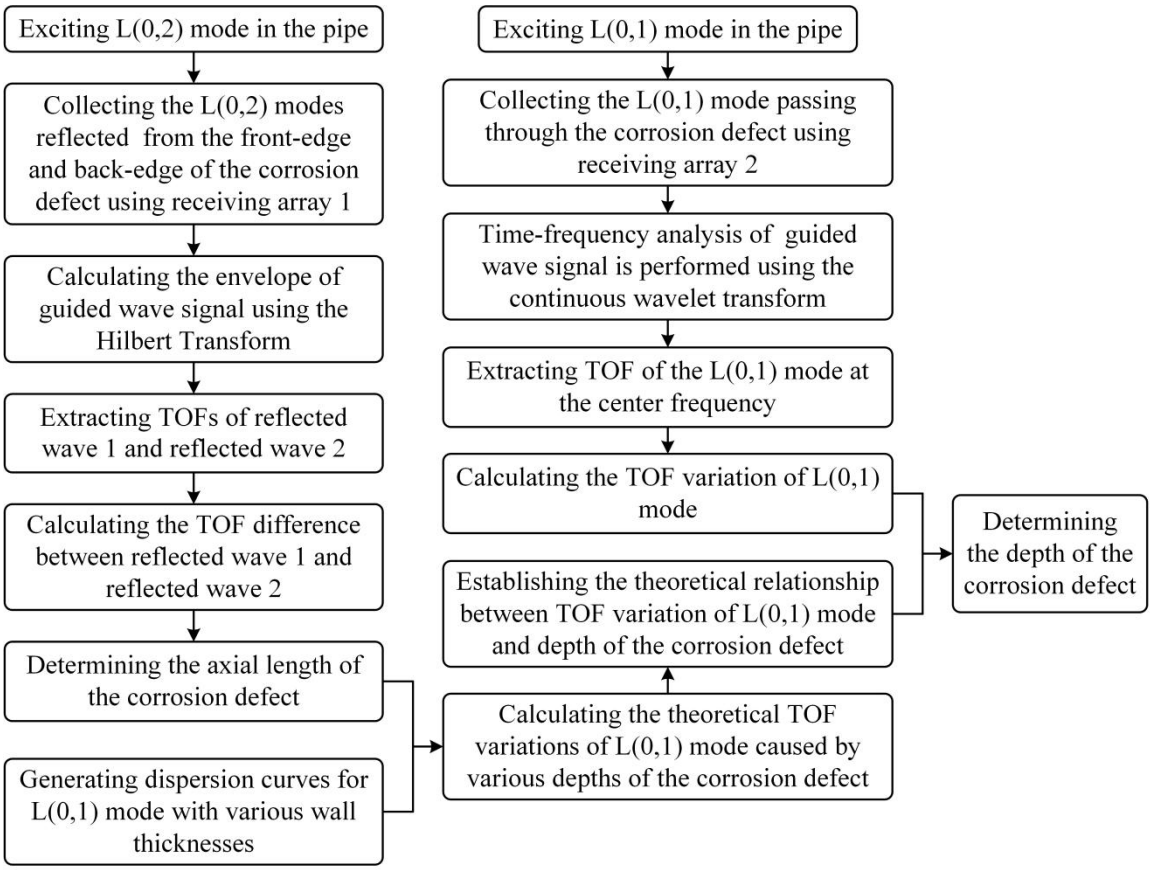
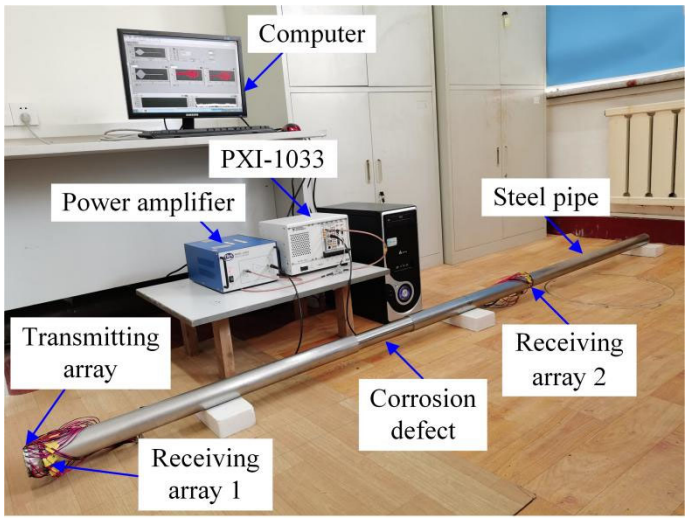


Figure 7. Flow chart for quantitative detection of full-circumferential localized corrosion defect in the pipe.

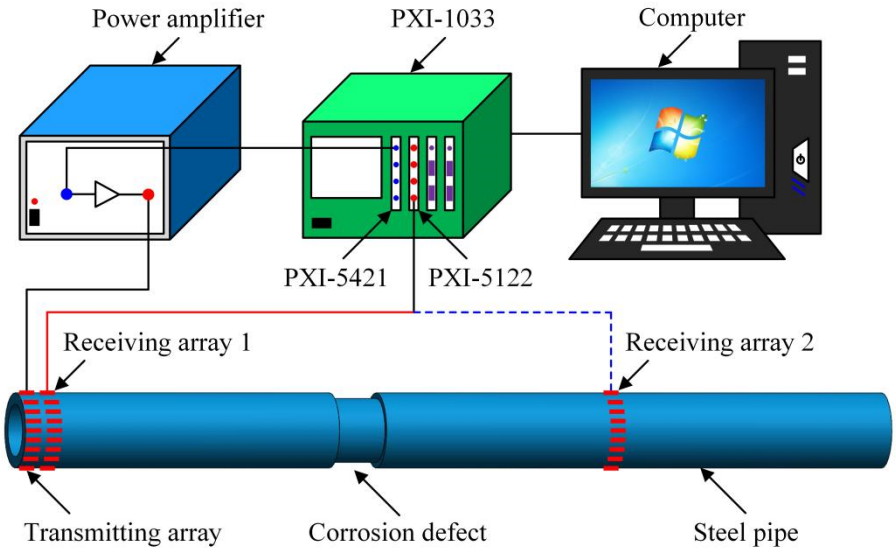
3. Experimental Study

To validate the effectiveness of the proposed method, experiments were conducted to detect full-circumferential localized corrosion defects in pipes. The test specimen was a steel pipe with a length of 2.88 m, an outer diameter of 59 mm, and a wall thickness of 7 mm. Piezoelectric lead zirconate titanate (PZT) transducers with dimensions of 20 × 5 × 1 mm were used as transmitters and receivers. The transmitting array was located at the left end of the pipe, and two sets of independent receiving arrays were installed at different positions: receiving array 1 was located at the right side of the transmitting array, and receiving array 2 was installed at a distance of 1.8 m from the left end of the pipe. Receiving array 1 was used to receive the L(0,2) modes reflected from the front-edge and back-edge of the corrosion defect, while receiving array 2 was used to receive the L(0,1) modes transmitted through the corrosion defect. When the number of transducers arranged at equal intervals along the circumference of the pipe in the transmitting array is greater than the highest order of the modes which can be present within the excitation frequency range, axisymmetric (circumferential order $n = 0$) modes can be efficiently excited and flexural modes can be effectively suppressed [33]. For the pipe used in this experiment, within the

excitation frequency range, the highest order of the mode was 7. In order to maximize the symmetry of the excitation and reception of guided waves, and reduce the circumferential asymmetry error caused by transducer adhesion deviation or material non-uniformity, 16 PZTs were used in the transmitting array, receiving array 1, and receiving array 2, respectively, for a total of 48 PZTs. The PZTs were longitudinal-extension type transducers, and the PZTs in the same array were evenly spaced along the circumference of the pipe. All PZTs in the excitation array were connected in parallel and simultaneously excited with the same amplitude. Thus, it can effectively generate the longitudinal modes and enhance the reliability of guided wave signal reception and the stability of experimental results. The PZTs in each receiving array independently acquired guided wave signals. To suppress potential interference from flexural modes, the signals received by individual PZTs within the same receiving array were averaged. The experimental setup is shown in Figure 8.



(**a**) Photograph of the experimental setup



(**b**) Schematic diagram of the experimental setup.

Figure 8. Experimental setup.

The excitation signals generated by the arbitrary waveform generator (PXI-5421) were amplified using a power amplifier (Trek 2100HF, TREK, Inc., Lockport, NY, USA) and then applied to the transmitting array to generate the desired guided wave modes in the pipe. The receiving arrays were connected to an oscilloscope (PXI-5122) for guided wave signal

acquisition, and the recorded signals were transferred to a computer for visualization and storage. LabVIEW program was used to set excitation signals, collect signals, and perform synchronization control. Both the PXI-5421 and PXI-5122 cards were integrated into a PXI-1033 chassis, and all three were manufactured by National Instruments (NI, Austin, TX, USA). The PXI-1033 chassis has 5 slots; the PXI-5421 has 16-bit resolution, a maximum update rate of 100 MS/s, and a bandwidth of 43 MHz; the PXI-5122 has 2 channels, a 14-bit resolution, a maximum sampling rate of 100 MS/s, and a bandwidth of 100 MHz. The Trek 2100HF has an output voltage range of 0 to $\pm$ 150 V and a voltage gain of 50 V/V.

For measurements using receiving array 1, the sampling frequency and acquisition time were set to 20 MHz and 1.2 ms, respectively. For receiving array 2, the corresponding parameters were set to 2 MHz and 1.7 ms, respectively. To excite the L(0,2) mode, a 7-cycle sine wave modulated by a Hanning window with center frequencies of 90 kHz and 100 kHz was employed. Under the same corrosion condition, the axial length of the corrosion defect was evaluated using the L(0,2) modes with these two center frequencies, respectively. For excitation of the L(0,1) mode, a 20-cycle sine wave modulated by a Hanning window was used. To determine an appropriate center frequency for L(0,1) mode excitation, frequencies ranging from 26 to 30 kHz were investigated with an interval of 0.5 kHz, and the quality of the received initial signals was evaluated. The experimental results showed that the L(0,1) mode signal exhibited a clear waveform, relatively high amplitude, and effective separation from end reflections at a center frequency of 28.5 kHz, facilitating accurate extraction of the TOF of the guided wave. When the center frequency exceeded 28.5 kHz, waveform overlap and distortion gradually appeared, resulting in degraded signal quality. Therefore, a 20-cycle sine wave modulated by a Hanning window with a center frequency of 28.5 kHz was selected for L(0,1) mode excitation. Full-circumferential localized corrosion defects were artificially fabricated on the pipe specimen by mechanical machining. The dimensions of the corrosion defects under different test conditions are listed in Table 1. Throughout the experiments, the axial starting position of the corrosion defects was maintained at a constant distance of 0.9 m from the left end of the pipe.

Table 1. Dimensions of the corrosion defects under different conditions.

Condition	Axial Length of Corrosion (mm)	Depth (mm)	Circumferential Angle (°)
1	170	1.5	360
2	210	1.5	360
3	210	2.5	360
4	210	3.5	360
5	210	4.5	360

The error in the measured axial length of the corrosion defect will affect the evaluation of the depth of the corrosion defect. In order to reduce the influence of the uncertainties in the quantitative results of the axial length of the corrosion defect on the quantification of the depth of the corrosion defect, the guided wave signals received by the receiving array 1 were tested repeatedly. When the center frequency of the excitation signal was 90 kHz and 100 kHz, the tests were repeated three times and five times, respectively. In the same corrosion condition, the axial length of the corrosion defect was evaluated using the guided wave signals from each test, and the average of the evaluation results at the same frequency was taken as the measured axial length of the corrosion defect. Since the excited L(0,2) mode is nearly non-dispersive, the effect of depth of corrosion defect on the TOF of the L(0,2) mode can be neglected, under each corrosion condition, the theoretical TOFs of reflected wave 1 at 90 kHz and 100 kHz were 3.40128×10^{-4} s and 3.40507×10^{-4} s, respectively. Under corrosion condition 1, the theoretical TOFs of reflected wave 2 at 90 kHz and 100 kHz were 4.04375×10^{-4} s and 4.04825×10^{-4} s, respectively; under corrosion conditions 2–5,

the theoretical TOFs of reflected wave 2 at 90 kHz and 100 kHz were 4.19492×10^{-4} s and 4.19959×10^{-4} s, respectively. Tables 2 and 3 present the measurement results of the TOF of reflected wave 1 and reflected wave 2. Under various corrosion conditions, the average values of TOFs of reflected wave 1 and reflected wave 2 measured by this method were consistent with their corresponding theoretical TOFs, with a maximum relative error of −3.29% and a small standard deviation. The guided wave signals received by receiving array 2 were tested once under each corrosion condition. In the initial state, the L(0,1) mode received by receiving array 2 was tested three times; the average value and standard deviation of the TOF of the L(0,1) mode measured by this method were 9.07×10^{-4} s and 5×10^{-7} s, respectively. The theoretical TOF of the L(0,1) mode in the initial state was 9.071×10^{-4} s. The average value of the TOF of the L(0,1) mode measured by this method was consistent with the theoretical TOF, and the standard deviation was small. These results indicate that the TOF calculation methods used in this study can effectively extract the TOF of the guided wave, suppress noise interference, and have good repeatability.

Table 2. Measurement results of the TOF of reflected wave 1.

Frequency (kHz)	Measurement Result	Condition				
		1	2	3	4	5
90	Average value(s)	3.28933×10^{-4}	3.29117×10^{-4}	3.2945×10^{-4}	3.2925×10^{-4}	3.2935×10^{-4}
	Standard deviation(s)	5.7735×10^{-8}	5.7735×10^{-8}	6.63936×10^{-20}	1×10^{-7}	7.07107×10^{-8}
100	Average value(s)	3.3047×10^{-4}	3.3032×10^{-4}	3.3038×10^{-4}	3.3017×10^{-4}	3.3022×10^{-4}
	Standard deviation(s)	2.73861×10^{-8}	2.73861×10^{-8}	4.47214×10^{-8}	1.03682×10^{-7}	4.47214×10^{-8}

Table 3. Measurement results of the TOF of reflected wave 2.

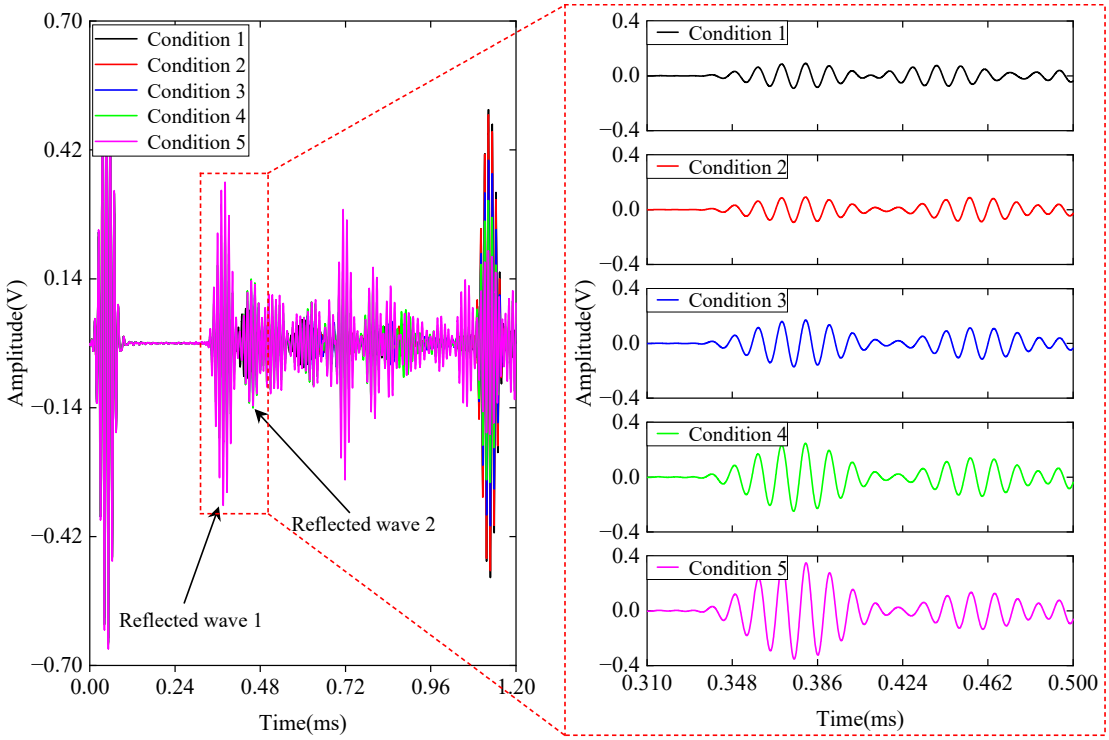
Frequency (kHz)	Measurement Result	Condition				
		1	2	3	4	5
90	Average value(s)	3.93233×10^{-4}	4.07667×10^{-4}	4.09567×10^{-4}	4.08867×10^{-4}	4.09×10^{-4}
	Standard deviation(s)	2.88675×10^{-7}	5.7735×10^{-8}	5.7735×10^{-8}	5.7735×10^{-8}	7.07107×10^{-8}
100	Average value(s)	3.9397×10^{-4}	4.0947×10^{-4}	4.0944×10^{-4}	4.1021×10^{-4}	4.1064×10^{-4}
	Standard deviation(s)	4.47214×10^{-8}	2.73861×10^{-8}	5.47723×10^{-8}	5.47723×10^{-8}	4.1833×10^{-8}

4. Experimental Results and Analysis

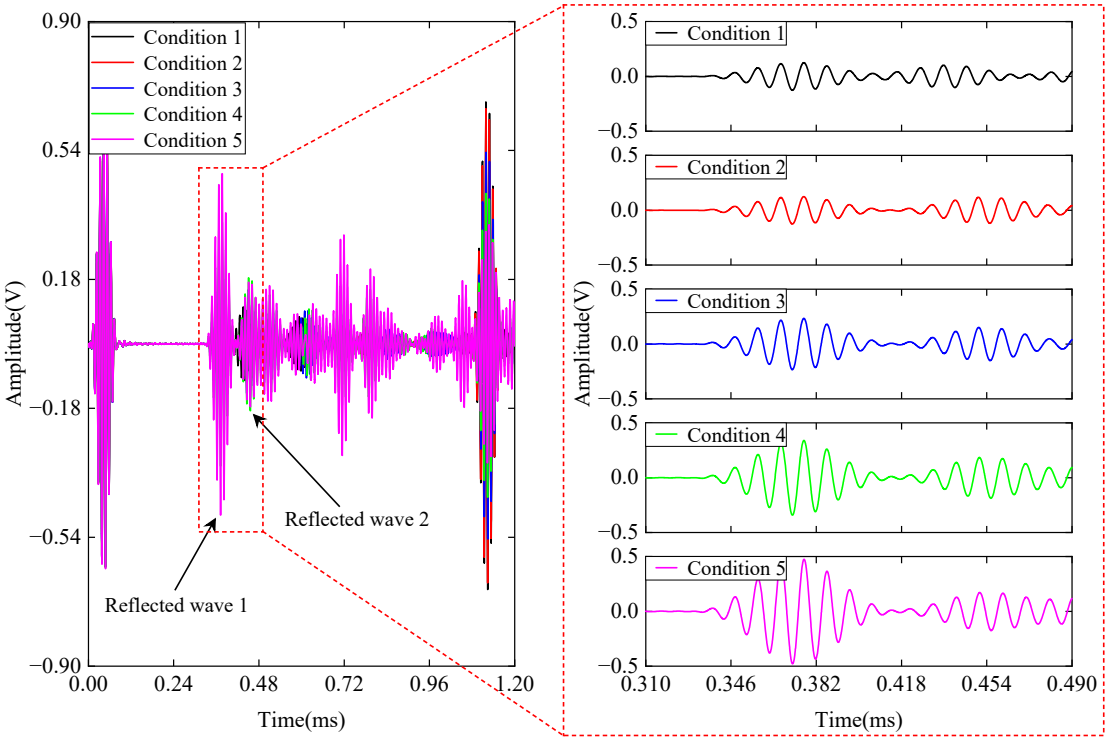
4.1. Quantitative Evaluation of Axial Length of Corrosion Defect

Figure 9 shows the guided wave signals acquired by receiving array 1 under different test conditions. When the incident L(0,2) mode propagates along the pipe and reaches the corrosion defect, reflected L(0,2) modes are generated from the front-edge and back-edge of the corrosion defect, respectively. As the axial length of the corrosion defect increases to the right side of the pipe, the TOF and amplitude of reflected wave 1 remain almost unchanged, indicating that, when reflected wave 1 and reflected wave 2 are effectively separated, the signal characteristics of reflection wave 1 are nearly unaffected by the increase in the axial length of the corrosion defect to the right side of the pipe. The amplitude of reflection wave 1 increases as the depth of the corrosion defect increases, indicating that a deeper corrosion defect enhances the energy of the reflected L(0,2) mode generated at the front-edge of the corrosion defect. Therefore, the amplitude of reflection wave 1 contains information related to the depth of the corrosion defect. The TOF of reflected wave 2 increases with the increase of the axial length of the corrosion defect to the right side of the pipe; therefore, the TOF difference of the L(0,2) modes reflected from the front-edge and back-edge of the corrosion defect can be used to quantify the axial length of the corrosion defect. When the center frequencies of the excitation signals were set to 90 and 100 kHz, respectively,

the received guided wave signals were almost identical, and reflected wave 1 exhibited the same variation trend with corrosion defect propagation. However, at the excitation frequency of 100 kHz, the amplitude of reflected wave 1 was higher than that at 90 kHz for the same corrosion depth, which improved the signal-to-noise ratio of the detected signals.



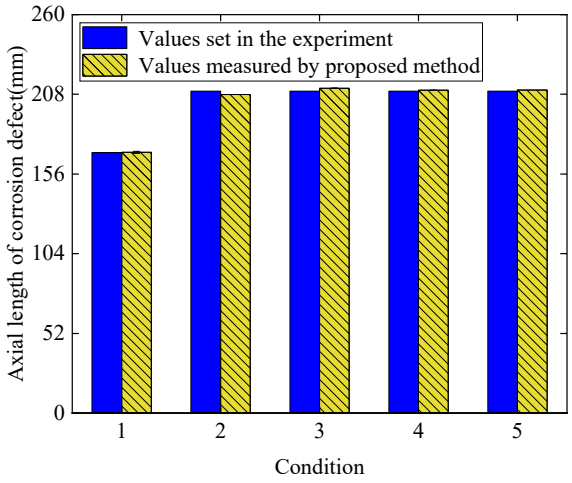
(**a**) 90 kHz



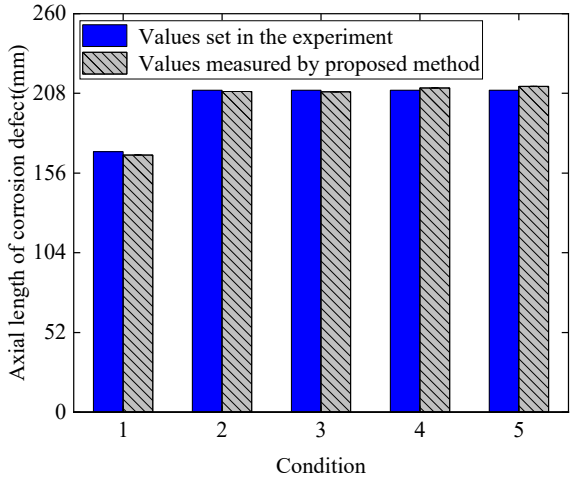
(**b**) 100 kHz

Figure 9. Guided wave signals obtained by receiving array 1 under different conditions.

The TOFs of reflected wave 1 and reflected wave 2 under different test conditions were further extracted, and the axial length of the corrosion defect was calculated using Equation (4), as shown in Figure 10. In the experiments, the axial length of the corrosion defect in condition 1 was set to 170 mm, while those in conditions 2–5 were all set to 210 mm. When the excitation center frequency was 90 kHz, the axial lengths of the corrosion defect obtained using the proposed method were 170.14, 207.85, 211.99, 210.67, and 210.76 mm, respectively. At the excitation center frequency of 100 kHz, the corresponding measured axial lengths of the corrosion defect were 167.84, 209.20, 208.96, 211.55, and 212.56 mm, respectively. The results show that the axial lengths of the corrosion defect measured by the proposed method agree well with the preset values, with a maximum relative error of −1.27%. This demonstrates that the proposed method can accurately quantify the axial length of full-circumferential localized corrosion defects.



(**a**) 90 kHz



(**b**) 100 kHz

Figure 10. Quantitative results of the axial length of the corrosion defect.

The TOF difference of the L(0,2) modes reflected from the front-edge and back-edge of the corrosion defect is positively correlated with the axial length of the corrosion defect. When the axial length of the corrosion defect allows the peak values of the reflected waves at both edges to be effectively distinguished, the axial length of the corrosion defect can be quantitatively evaluated directly using the proposed method. The defect dimensions in this study satisfy this condition. If the axial length of the corrosion defect is too short, it can lead to waveform overlap and make it difficult to distinguish the peak values of the

reflected waves from the two edges. In this case, signal processing methods such as the Hilbert-Huang transform [27] and matching pursuit [34] can be employed to separate the reflected waves, and the proposed method can then be combined with these techniques to perform quantitative detection of the axial length.

4.2. Quantitative Evaluation of Depth of Corrosion Defect

Figure 11 shows the L(0,1) mode signals acquired by receiving array 2 under the intact condition and different corrosion conditions. When a corrosion defect is introduced, the guided wave signals shift toward the left, which is attributed to the reduction in pipe wall thickness caused by corrosion. The reduced wall thickness increases the group velocity of the L(0,1) mode, thereby shortening its TOF. The experimental observations are in good agreement with the theoretical analysis. For the same corrosion depth, the TOF of the L(0,1) mode decreases with the increase of the axial length of the corrosion defect. This is because the increase in the axial length of the corrosion defect leads to the extension of the length of the region where the group velocity of the L(0,1) mode increases, which in turn causes the TOF of the L(0,1) mode to gradually decrease. Therefore, the TOF variation of the L(0,1) mode is positively correlated with the axial length of the corrosion defect. For the same axial length of the corrosion defect, the TOF of the L(0,1) mode decreases as the depth of the corrosion defect increases. This is because a deeper corrosion defect further increases the group velocity of the L(0,1) mode within the defect region, leading to a continuous reduction in TOF. Since both axial length and depth of the corrosion defect contribute to the decrease in the TOF of the L(0,1) mode, the TOF variation of the L(0,1) mode contains information about both defect parameters. Therefore, once the axial length of the corrosion defect is determined, the TOF variation of the L(0,1) mode can be used for quantitative evaluation of the depth of the corrosion defect.

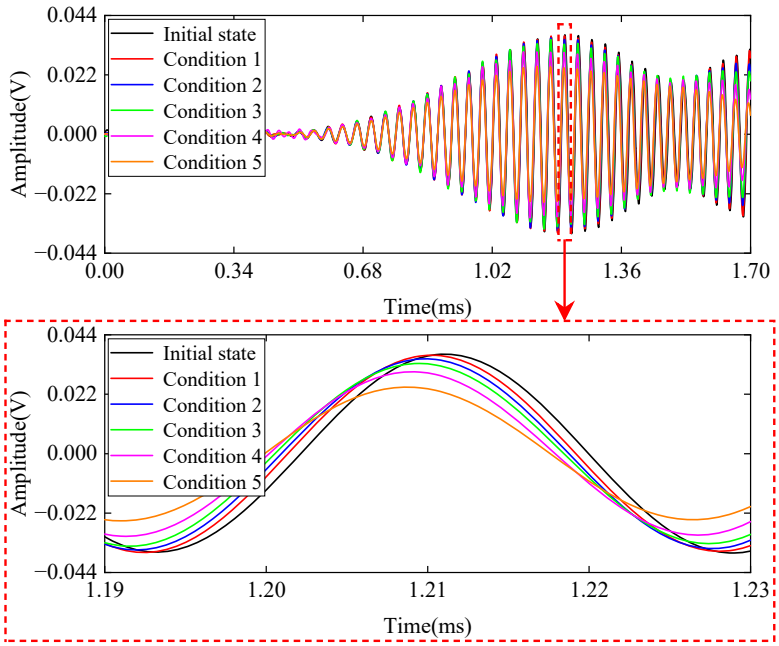
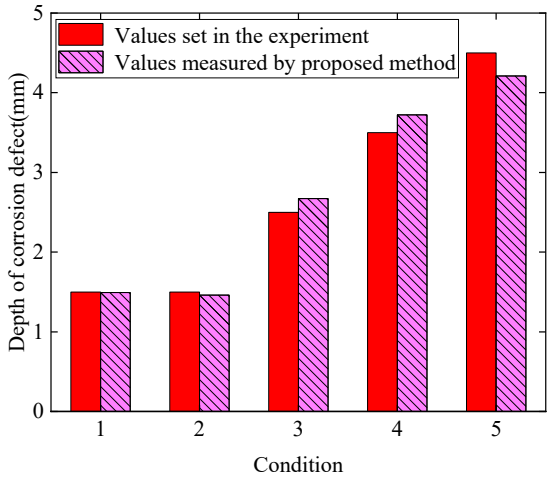


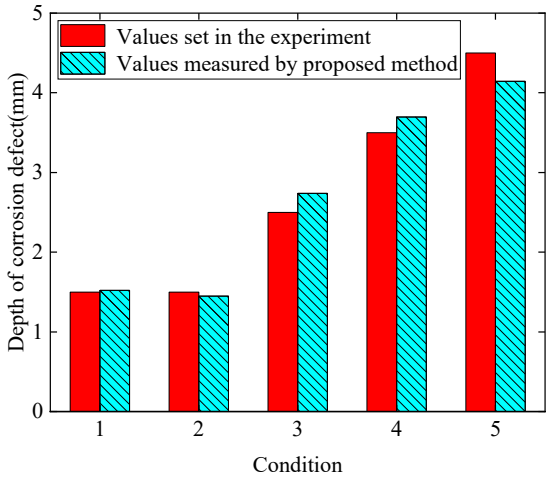
Figure 11. L(0,1) modes obtained by receiving array 2 in the initial state and under different corrosion conditions.

Based on the axial lengths of the corrosion defect measured under different corrosion conditions in Section 4.1, the depths of the corrosion defect under different corrosion conditions were further evaluated using the proposed quantitative estimation method for the depth of the corrosion defect. The measured results were compared with the preset

values, as shown in Figure 12. The depths of the corrosion defect set in the experiment were 1.5, 1.5, 2.5, 3.5, and 4.5 mm, respectively. When the center frequency used for detecting the axial lengths of the corrosion defect was 90 kHz, the depths of the corrosion defect measured using the proposed method under different corrosion conditions were 1.494, 1.461, 2.671, 3.723, and 4.210 mm, respectively. When the center frequency used for detecting the axial lengths of the corrosion defect was 100 kHz, the corresponding measured depths of the corrosion defect were 1.522, 1.448, 2.738, 3.696, and 4.144 mm, respectively. The results show that the measured depths of the corrosion defect are in good agreement with the preset values, with a maximum relative error of 9.52%. Therefore, the proposed method can accurately quantify the depth of the corrosion defect.



(**a**) The center frequency for detecting the axial length of the corrosion defect was 90 kHz



(**b**) The center frequency for detecting the axial length of the corrosion defect was 100 kHz

Figure 12. Quantitative results of the depth of the corrosion defect.

4.3. Sensitivity Analysis of Depth Estimation to the Accuracy of Axial Length Measurement

The sensitivity of depth estimation to the accuracy of axial length measurement was analyzed. Taking a center frequency of 90 kHz for the excitation signal as an example, assuming that the relative errors of the axial length measurement of the corrosion defect were 1%, 3%, 5%, and 7%, respectively, the measurement results of the depth of the corrosion defect under different relative errors were analyzed, as shown in Table 4. The relative error in the measurement of the axial length of the corrosion defect in the table was denoted by RE_L. The measured depth of the corrosion defect decreases with the increase of RE_L. The evaluation results for the depth of the corrosion defect at RE_L = 1% were used as a reference. When the relative error in depth measurement was positive, the absolute

value of the relative error in depth measurement first decreased and then increased as RE_L increased; when the relative error in depth measurement was negative, the absolute value of the relative error in depth measurement continued to increase as RE_L increased. In these four cases, the maximum errors of depth evaluation of corrosion defect were −7.56%, −11.11%, −14.44% and −17.56%, respectively; The increase rate of the absolute value of the maximum relative error in depth measurement was slightly greater than that of RE_L. These results indicate that the estimation of the depth of corrosion defects is somewhat sensitive to RE_L. Therefore, to improve the accuracy and robustness of depth assessment of corrosion defects, the accuracy of axial length measurement of corrosion defects should be ensured as much as possible.

Table 4. Measurement results for depth of corrosion defect at different relative errors in the measurement of axial length of corrosio defect.

Actual Δd_c(mm)	RE_L = 1%		RE_L = 3%		RE_L = 5%		RE_L = 7%	
	Measured Δd_c (mm)	Relative Error (%)	Measured Δd_c (mm)	Relative Error (%)	Measured Δd_c (mm)	Relative Error (%)	Measured Δd_c	Relative Error (%)
1.5	1.48	−1.33	1.44	−4.00	1.41	−6.00	1.37	−8.67
1.5	1.42	−5.33	1.39	−7.33	1.35	−10.00	1.32	−12.00
2.5	2.67	6.80	2.59	3.60	2.51	0.40	2.44	−2.40
3.5	3.68	5.14	3.54	1.14	3.42	−2.29	3.30	−5.71
4.5	4.16	−7.56	4.00	−11.11	3.85	−14.44	3.71	−17.56

5. Discussion

In this study, the effectiveness of the proposed method was validated using five defect conditions in a single steel pipe. The interaction mechanism between the L(0,1) and L(0,2) modes and full-circumferential localized corrosion in commonly used metal pipes under different wall thicknesses and materials is approximated. The dispersion characteristics of the L(0,1) mode are influenced by wall thickness and diameter. For a given wall thickness, the highest frequency within the frequency range where only the L(0,1) mode exists in the longitudinal modes decreases as the pipe diameter increases. If the highest frequency is too low, it is difficult to excite guided waves. Therefore, for a given pipe, the dispersion curve should be analyzed first to determine an excitation frequency that can effectively excite the pure L(0,1) mode, and then the proposed method can be used to detect the axial length and depth of full-circumferential localized corrosion.

The proposed method has only been proven to be able to quantitatively detect full-circumferential localized corrosion defects in pipes. When a guided wave encounters a part-circumferential localized corrosion defect, more complex reflections, transmissions, and mode conversions occur because of the circumferential discontinuity of the defect in the pipe, leading to multimode aliasing and increasing the difficulty of mode identification. To effectively detect such defects, it is still necessary to conduct in-depth research into the interaction mechanisms between these defects and ultrasonic guided waves and to develop signal processing methods with superior performance. When irregularities in the corrosion profile or nonuniform loss of wall thickness reach a certain level, they can cause complex phenomena such as reflection, scattering, and mode conversion, leading to multimode aliasing, which reduces the accuracy of mode identification and affects the accuracy of the proposed method. Rough surfaces primarily exacerbate the energy dissipation of guided waves; since the proposed method is based on TOF rather than amplitude, the quantitative determination of axial length and depth is not sensitive to surface roughness as long as the signal can be effectively identified. However, excessive roughness significantly weakens the signal and increases interference during TOF extraction, thereby affecting the reliability of the proposed method. We plan to systematically investigate the impact of

irregular corrosion profiles, non-uniform wall thickness loss, and surface roughness levels on guided wave propagation and detection accuracy of the proposed method through theory, experiments, and finite element simulations in the future.

In this study, all corrosion defects were artificially manufactured by mechanical processing, and there were no corrosion degradation products in the pipe. Pipe corrosion usually produces corrosion degradation products, but in actual engineering, whether these degradation products form deposits depends on factors such as the solubility of corrosion products, the composition and flow state of the medium, and the surface condition of the pipe. If the degradation products do not form significant deposits, or if the acoustic impedance of the deposits formed by the degradation products is significantly different from that of the pipe, it will have little effect on the proposed method. If the acoustic impedance of the resulting deposits is similar to that of the pipe material, the deposits may alter the propagation characteristics of guided waves and consequently affect the detection accuracy of the proposed method. In the future, further research can be conducted on the impact of actual degradation products on the propagation characteristics of guided waves and the proposed method.

6. Conclusions

A new detection method for simultaneous quantification of axial length and depth of full-circumferential localized corrosion in pipes is proposed based on a fusion strategy of pulse-echo and pitch-catch methods. First, the theoretical relationship between the TOF difference of the L(0,2) modes reflected from the front-edge and back-edge of the corrosion defect and the axial length of the corrosion defect was established based on the pulse-echo method, enabling quantitative evaluation of the axial length of the corrosion defect. Subsequently, with the axial length of the corrosion defect determined, the theoretical relationship between the TOF variation of the L(0,1) mode and the depth of the corrosion defect was established using the pitch-catch method, achieving quantitative evaluation of the depth of the corrosion defect. Experimental investigations were conducted to validate the proposed method. The main conclusions are as follows:

(1) The TOF difference between reflected wave 1 and reflected wave 2 increases as the axial length of the corrosion defect increases. The axial length of the corrosion defect can be quantitatively identified using the established theoretical relationship between the TOF difference of the L(0,2) modes reflected from the front-edge and back-edge of the corrosion defect and the axial length of the corrosion defect.

(2) The TOF variation of the L(0,1) mode contains information on both the axial length and depth of the corrosion defect; after the axial length of the corrosion defect is quantified, the depth of the corrosion defect can be effectively quantified using the established theoretical relationship between the TOF variation of the L(0,1) mode and the depth of the corrosion defect.

(3) The axial lengths and depths of the full-circumferential localized corrosion defects measured by this method are consistent with the predefined defect dimensions, with maximum relative errors of −1.27% and 9.52%, respectively. The proposed method addresses a limitation of conventional guided wave techniques, which generally have difficulty in accurately quantifying both the axial length and depth of full-circumferential localized corrosion defects simultaneously.

Author Contributions: Conceptualization, Y.L.; methodology, Y.L. and X.F.; software, Y.L. and L.S.; validation, Y.L., H.H., L.S. and X.F.; formal analysis, Y.L. and L.S.; investigation, Y.L., L.S. and X.F.; resources, X.F., H.H. and G.C.; data curation, Y.L.; writing—original draft preparation, Y.L., H.H. and L.S.; writing—review and editing, H.H. and G.C.; visualization, Y.L. and L.S.; supervision, H.H., X.F.

and G.C.; project administration, G.C.; funding acquisition, H.H., G.C. and X.F. All authors have read and agreed to the published version of the manuscript.

Funding: This work was supported by the National Natural Science Foundation of China (Grant No. 52079024), the Fundamental Research Funds for IWHR (SM0145B042021, SM110145B0012025), and the Open Research Fund of State Key Laboratory of Water Cycle and Water Security, China Institute of Water Resources and Hydropower Research (SKL2024YJTS14).

Institutional Review Board Statement: Not applicable.

Informed Consent Statement: Not applicable.

Data Availability Statement: The data presented in this study are available on request from the corresponding author.

Conflicts of Interest: The authors declare no conflicts of interest.

References

1. Zang, X.; Xu, Z.-D.; Lu, H.; Zhu, C.; Zhang, Z. Ultrasonic guided wave techniques and applications in pipeline defect detection: A review. *Int. J. Press. Vessel. Pip.* **2023**, *206*, 105033. [CrossRef]
2. Zhu, W.; Chen, R.; Chen, C.; Fu, Y.; Wu, L.; Yan, Y.; An, Y.; Yin, W.; Qu, Z. An Eco-friendly Crystal Scales Removal Technique of Fluid Transmission Pipes with Various Flow Types and Void Fractions Using Ultrasonic Guided Waves. *Chem. Eng. Process.-Process Intensif.* **2026**, *228*, 110973. [CrossRef]
3. Kahnamouei, J.T.; Moallem, M. A comprehensive review of in-pipe robots. *Ocean Eng.* **2023**, *277*, 114260. [CrossRef]
4. Yeshanew, D.A.; Jiru, M.G.; Ahmed, G.M.S.; Badruddin, I.A.; Soudagar, M.E.M.; Kamangar, S.; Tolcha, M.A. Corrosion characterization at surface and subsurface of iron-based buried water pipelines. *Materials* **2021**, *14*, 5877. [CrossRef] [PubMed]
5. Ahmad, Z. *Principles of Corrosion Engineering and Corrosion Control*; Elsevier: Amsterdam, The Netherlands, 2007.
6. Demma, A.; Cawley, P.; Lowe, M.; Roosenbrand, A.; Pavlakovic, B. The reflection of guided waves from notches in pipes: A guide for interpreting corrosion measurements. *NDT E Int.* **2004**, *37*, 167–180. [CrossRef]
7. Wang, X.; Peter, W.T.; Mechefske, C.K.; Hua, M. Experimental investigation of reflection in guided wave-based inspection for the characterization of pipeline defects. *NDT E Int.* **2010**, *43*, 365–374. [CrossRef]
8. Ma, Q.; Tian, G.; Zeng, Y.; Li, R.; Song, H.; Wang, Z.; Gao, B.; Zeng, K. Pipeline in-line inspection method, instrumentation and data management. *Sensors* **2021**, *21*, 3862. [CrossRef] [PubMed]
9. Li, Y.; Sun, C.; Liu, Y. Magnetic flux leakage testing method for pipelines with stress corrosion defects based on improved kernel extreme learning machine. *Electronics* **2023**, *12*, 3707. [CrossRef]
10. Fang, J.; Shen, J.; Xiong, L.; Yang, K.; Din, Z.; Meng, Z.; Yin, W.; Xiao, S. Modelling and experimental study on pipeline defect characterisations using a pulsed eddy current measurement. *Nondestruct. Test. Eval.* **2025**, *40*, 4024–4045. [CrossRef]
11. Cherqaoui, B.; Henneron, T.; Tang, Z.; Ducreux, J.-P.; Guillot, E.; Clénet, S. Finite element modeling of real defects in thin-walled tubes derived from X-ray tomography. *NDT E Int.* **2026**, *164*, 103833. [CrossRef]
12. Peng, K.; Zhang, Y.; Xu, X.; Han, J.; Luo, Y. Crack detection of threaded steel rods based on ultrasonic guided waves. *Sensors* **2022**, *22*, 6885. [CrossRef] [PubMed]
13. Xing, H.; Di, W.; Sun, X.; Wang, M.; Li, C. Bolt anchorage defect identification based on ultrasonic guided wave and deep learning. *Sensors* **2025**, *25*, 6431. [CrossRef] [PubMed]
14. Sun, X.; Zhang, M.; Gao, W.; Guo, C.; Kong, Q. A novel method for steel bar all-stage pitting corrosion monitoring using the feature-level fusion of ultrasonic direct waves and coda waves. *Struct. Health Monit.* **2023**, *22*, 714–729. [CrossRef]
15. Xu, X.; Tu, J.; Yun, C.B.; Duan, Y.-F. Ultrasonic guided waves-based fatigue crack detection in a steel I-beam: An experimental study. *Smart Struct. Syst.* **2022**, *31*, 13–27.
16. Li, Q.; Luo, Z.; Zhou, S. Novel baseline-free ultrasonic Lamb wave defect location method based on path amplitude matching. *Meas. Sci. Technol.* **2024**, *35*, 065111. [CrossRef]
17. Jagadeeshwar, T.L.; Kalyani, S.; Rajagopal, P.; Srinivasan, B. Statistics-based baseline-free approach for rapid inspection of delamination in composite structures using ultrasonic guided waves. *Struct. Health Monit.* **2022**, *21*, 2719–2731. [CrossRef]
18. Yang, Z.; Yang, H.; Tian, T.; Deng, D.; Hu, M.; Ma, J.; Gao, D.; Zhang, J.; Ma, S.; Yang, L. A review on guided-ultrasonic-wave-based structural health monitoring: From fundamental theory to machine learning techniques. *Ultrasonics* **2023**, *133*, 107014. [CrossRef] [PubMed]
19. Cawley, P. Guided waves in long range nondestructive testing and structural health monitoring: Principles, history of applications and prospects. *NDT E Int.* **2024**, *142*, 103026. [CrossRef]

20. Abuassal, A.; Kang, L.; Martinho, L.; Kubrusly, A.; Dixon, S.; Smart, E.; Ma, H.; Sanders, D. A review of recent advances in unidirectional ultrasonic guided wave techniques for nondestructive testing and evaluation. *Sensors* **2025**, *25*, 1050. [CrossRef] [PubMed]
21. Memon, A.M.; Alhems, L.M. Applications of EMAT generated guided waves in pipes: A review. *E-J. Nondestr. Test.* **2023**, *28*, 1435–4934. [CrossRef] [PubMed]
22. Cawley, P.; Lowe, M.; Simonetti, F.; Chevalier, C.; Roosenbrand, A. The variation of the reflection coefficient of extensional guided waves in pipes from defects as a function of defect depth, axial extent, circumferential extent and frequency. *Proc. Inst. Mech. Eng. Part C J. Mech. Eng. Sci.* **2002**, *216*, 1131–1143. [CrossRef]
23. Zhu, W. An FEM simulation for guided elastic wave generation and reflection in hollow cylinders with corrosion defects. *J. Press. Vessel Technol.* **2002**, *124*, 108–117. [CrossRef]
24. Demma, A.; Cawley, P.; Lowe, M.; Roosenbrand, A. The reflection of the fundamental torsional mode from cracks and notches in pipes. *J. Acoust. Soc. Am.* **2003**, *114*, 611–625. [CrossRef] [PubMed]
25. Zhang, X.; Zhou, J.; Li, Y. Time-reversal fusion technology via waveform coupling for detecting defects in cross-pipeline weld short supports. *Measurement* **2025**, *261*, 119871. [CrossRef]
26. Zhang, H.; Teng, F.; Wei, J.; Lv, S.; Zhang, L.; Zhang, F.; Jiang, M. Damage location method of pipeline structure by ultrasonic guided wave based on probability fusion. *IEEE Trans. Instrum. Meas.* **2024**, *73*, 9504914. [CrossRef]
27. Wang, X.; Tse, P.W.; Dordjevich, A. Evaluation of pipeline defect's characteristic axial length via model-based parameter estimation in ultrasonic guided wave-based inspection. *Meas. Sci. Technol.* **2011**, *22*, 025701. [CrossRef]
28. Gazis, D.C. Three-dimensional investigation of the propagation of waves in hollow circular cylinders. *I. Anal. Found. J. Acoust. Soc. Am.* **1959**, *31*, 568–573. [CrossRef]
29. Pavlakovic, B.; Lowe, M.; Alleyne, D.; Cawley, P. Disperse: A general purpose program for creating dispersion curves. In *Review of Progress in Quantitative Nondestructive Evaluation*; Thompson, D.O., Chimenti, D.E., Eds.; Plenum Press: New York, NY, USA, 1997; pp. 185–192.
30. Rose, J.L. *Ultrasonic Waves in Solid Media*; Cambridge University Press: New York, NY, USA, 1999.
31. Zheng, Y.B.; Liu, K.H.; Wu, Z.J.; Gao, D.Y.; Gorgin, R.; Ma, S.Y.; Lei, Z.K. Lamb waves and electro-mechanical impedance based damage detection using a mobile PZT transducer set. *Ultrasonics* **2019**, *92*, 13–20. [CrossRef] [PubMed]
32. Rioul, O.; Vetterli, M. Wavelets and signal processing. *IEEE Signal Process. Mag.* **1991**, *8*, 14–38. [CrossRef]
33. Lowe, M.J.S.; Alleyne, D.N.; Cawley, P. Defect detection in pipes using guided waves. *Ultrasonics* **1998**, *36*, 147–154. [CrossRef]
34. Tse, P.W.; Wang, X.J. Characterization of pipeline defect in guided-waves based inspection through matching pursuit with the optimized dictionary. *NDT E Int.* **2013**, *54*, 171–182. [CrossRef]

Disclaimer/Publisher's Note: The statements, opinions and data contained in all publications are solely those of the individual author(s) and contributor(s) and not of MDPI and/or the editor(s). MDPI and/or the editor(s) disclaim responsibility for any injury to people or property resulting from any ideas, methods, instructions or products referred to in the content.